Double photoionization of helium: Use of a correlated two-electron continuum wave function

M. A. Kornberg and J. E. Miraglia

Instituto de Astronomía y Física del Espacio, Consejo Nacional de Investigaciones Científicas y Técnicas, Casilla de Correo No. 67, Sucursal 28, 1428 Buenos Aires, Argentina

(Received 1 June 1993)

A correlated two-electron continuum wave function satisfying the correct asymptotic boundary condition is used to calculate double-photoionization cross sections. It is built up as a product of three two-body Coulomb continua. As a highly correlated ground-state wave function is employed, the present results serve as a critical test of the two-electron continuum wave function on this double process. For all energies, the results exhibit a large discrepancy between the length and velocity forms. In the high-energy limit, the velocity form agrees quite well with recent synchrotron measurements and with previous calculations. At low photon energies, the approximation fails to account for the data in magnitude and shape.

PACS number(s): 32.80.Fb, 32.30.Rj

I. INTRODUCTION

Double photoionization of helium stands as a fundamental problem for understanding the effects of electron-electron interaction (see [1] for a review). Since the helium ground-state wave function can be obtained with high accuracy, the key problem on the theoretical front rests in the solution of the final continuum state of the three-body problem interacting via Coulomb potentials.

It is infrequent to find in the literature manageable expressions for double-continuum wave functions with certain degree of reliability. We can mention here the independent-electron approximation which neglects correlation, the Hartree-Fock continuum with different options of effective charges [2, 3], the classical description of two electrons slowly escaping in the Wannier theory [4], and the asymptotic expressions as the particles are far apart [5].

We will here concentrate on a final state which is built as a simple product of three two-body Coulomb continua [Eq. (6) below]. This distorted wave function was initially posed in the 1960s to deal with excitation in electron-hydrogen collisions [6]; later on it was extended to ionization in the context of ion-atom collisions [7]. More recently it has been studied by Briggs and collaborators in the context of electron-impact ionization [8–10], in double-ionization of helium by fast electrons [11], and in the calculation of the asymmetry parameter for double photoionization [12].

To test the theory, there are several double-photoionization measurements of total cross sections at low [13–18] and high [19,20] photon energies. Also, single differential cross sections are available [14], which represent a further demand for the theory to unfold.

Atomic units will be employed throughout this work except where otherwise explicitly stated.

II. THEORY

A. Double differential cross section

The process that we consider is the impact of one linearly polarized photon on helium atoms in their ground state. For double photoionization to occur the photon energy (E_γ) must be greater than $-E_0$, where E_0 is the ground-state energy. Above the double ionization threshold, the ejection of both electrons may take place, with energies ε_1 and ε_2 related to the photon and ground state energies through the conservation law $E_\gamma + E_0 = \varepsilon_1 + \varepsilon_2$.

The matrix element of interest is

$$\mathbf{T}_{fi}^{(G)}(\mathbf{k}_1, \mathbf{k}_2) = \langle \psi_f^- | \mathbf{O}^{(G)} | \psi_i \rangle, \tag{1}$$

where the operator $\mathbf{O}^{(G)}$ is the matter-radiation interaction in the dipole approximation, which can be calculated in its three different gauges, namely, $\mathbf{O}^{(L)} = \mathbf{r}_1 + \mathbf{r}_2$, $\mathbf{O}^{(V)} = \nabla_1 + \nabla_2$, and $\mathbf{O}^{(A)} = Z_T \mathbf{r}_1 / r_1^3 + Z_T \mathbf{r}_2 / r_2^3$, where L, V, and A denote the length, velocity, and acceleration gauges respectively; and Z_T is the nuclear charge ($Z_T = 2$ for helium). In Eq. (1) $\psi_i(^1S_0|\mathbf{r}_1, \mathbf{r}_2)$ is the initial ground-state wave function and $\psi_f^-(\mathbf{k}_1, \mathbf{k}_2|\mathbf{r}_1, \mathbf{r}_2)$ is the final double-continuum-state wave function.

The most detailed observable of the double-photoionization process is the fifthfold differential cross section (FDCS) $d^5\sigma^{2+}/d\varepsilon_1 d\Omega_1 d\Omega_2$, where ε_1 is the energy of one of the electrons whose momentum $\mathbf{k}_1$ subtends an element of solid angle $d\Omega_1$. The quantities labeled with 2 refer to the other electron. Therefore [21]

$$\frac{d^5\sigma^{2+\ (G)}}{d\varepsilon_1 d\Omega_1 d\Omega_2} = (4\pi^2 \alpha a_0^2) k_1 k_2 C^{(G)} |\hat{\mathbf{e}} \cdot \mathbf{T}_{fi}^{(G)}(\mathbf{k}_1, \mathbf{k}_2)|^2, \tag{2}$$

where $C^{(L)} = E_\gamma$, $C^{(V)} = E_\gamma^{-1}$, and $C^{(A)} = E_\gamma^{-3}$, for the length, velocity, and acceleration gauges, respectively. The unit vector $\hat{\mathbf{e}}$ is the photon polarization direction (usually along the z axis). In Eq. (2), α is the fine-structure constant, a_0 the Bohr radius, and the final-state wave function is assumed to be normalized to the δ function in the momentum space. The length, velocity, and acceleration forms of the FDCS give the same result if both the initial and final wave functions are exact solutions of the three-body Hamiltonian.

In what follows, we perform three integrals in closed form to arrive at a double differential cross section (DDCS) $d^2\sigma^{2+}/d\varepsilon_1 \sin\theta_{12} d\theta_{12}$, describing the electron energy spectrum and the relative angle distribution, as was developed in Ref. [22]. If we exploit the fact that the inner product is rotationally invariant, angular integrations of the FDCS may be easily performed. In the original coordinate system xyz vectors $\mathbf{k}_1$ and $\mathbf{k}_2$ have polar angles θ_1, ϕ_1 and θ_2, ϕ_2, respectively. We can perform a rotation defined by Euler angles [24] $\alpha = \phi_1$, $\beta = \theta_1$, and $\gamma = 0$, so that in the rotated system $x'y'z'$, $\mathbf{k}_1$ is along the z' direction and $\mathbf{k}_2$ has polar angles θ_2', ϕ_2'. A subsequent rotation of the coordinate system with Euler angles $\alpha' = \phi_2'$, $\beta' = 0$, and $\gamma' = 0$ leads the new system to $x''y''z''$, where $\mathbf{k}_1$ is in the z'' direction and $\mathbf{k}_2$ is in the $x''z''$ plane. Angle θ_{12}, taken to be the asymptotic angle between $\mathbf{k}_1$ and $\mathbf{k}_2$, is now simply θ_2''. Taking into account that the solid-angle element is rotationally invariant, it may be easily shown that

$$\int\int |\hat{\mathbf{e}}'' \cdot \mathbf{T}_{fi}^{(G)''}|^2 d\Omega_1 d\phi_2' = \frac{8\pi^2}{3} |\mathbf{T}_{fi}^{(G)}|^2, \tag{3}$$

and the DDCS reads

$$\frac{d^2\sigma^{2+\ (G)}}{d\varepsilon_1 \sin\theta_{12} d\theta_{12}} = (4\pi^2 \alpha a_0^2) k_1 k_2 C^{(G)} \left(\frac{8\pi^2}{3}\right) |\mathbf{T}_{fi}^{(G)}|^2. \tag{4}$$

The single differential cross sections are obtained numerically by integrating the DDCS in the usual way. One further numerical integration is required to obtain the total cross section; on doing this, it must be considered that the correctly normalized total cross section is one half of the integral in the shake-off region [14, 21]. The DDCS here presented differs from that developed in Refs. [4, 12]. In that case, $d^2\sigma^{2+}/d\varepsilon_1 \sin\theta_1 d\theta_1$ is calculated instead, from which the asymmetry parameter β is extracted. Our procedure in turn offers a more practical way to integrate the FDCS.

B. Initial state wave functions

On going beyond the independent-particle model (Hartree-Fock) for the ground state of the helium atom we have used two wave functions developed by Bonham and Kohl [25] given by

$$\psi_i(\mathbf{r}_1, \mathbf{r}_2) = N_i (e^{-ar_1} e^{-br_2} + e^{-br_1} e^{-ar_2})(1 + C_0 e^{-\lambda_0 r_{12}}). \tag{5}$$

It is important to note that the correlation energy of the initial state plays a fundamental role in the description of the double-photoionization process [21, 23]. In the asymptotic limit Åberg [26] has shown that the accuracy of the results depends crucially on the fulfillment of the cusp condition at the nucleus. For helium, this condition is equal to $R_{\rm cusp} = (\partial\psi/\partial r_2)_{r_2=0}/\psi(r_1, r_2 = 0) = -2$. If the initial-state wave function deviates from $R_{\rm cusp} = -2$, the results can vary substantially. Table I shows the parameters of two wave functions—labeled with GS1 and GS2—with the values of the correlation energies and the cusp ratios. Also, a multiconfigurational self-consistent-field wave function developed by Sabelli and Hinze (SH) [27] ($E_{\rm corr} = 98\%$, $R_{\rm cusp} = -2.161$) was used to contrast our findings.

C. Final-state wave functions

The final-state wave function that we used here—which we call continuum product of three Coulomb waves (C3)—reads [7–10]

$$\psi_f^-(\mathbf{k}_1, \mathbf{k}_2 | \mathbf{r}_1, \mathbf{r}_2) = \mathcal{P}_{12} \psi_{\mathbf{k}_1}^-(Z_T; \mathbf{r}_1) \psi_{\mathbf{k}_2}^-(Z_T; \mathbf{r}_2) \times D^-(\xi_{12}, \mathbf{k}_{12};\ \mathbf{r}_{12}), \tag{6}$$

where $\psi_{\mathbf{k}}^-(Z; \mathbf{r}) = \psi_{\mathbf{k}}^0(\mathbf{r}) D^-(\xi, \mathbf{k}; \mathbf{r})$ is the Coulomb continuum wave function, $\psi_{\mathbf{k}}^0(\mathbf{r}) = \exp(i\mathbf{k}\cdot\mathbf{r})/(2\pi)^{(3/2)}$ is the free plane wave,

$$D^-(\xi, \mathbf{k}; \mathbf{r}) = N(\xi)\, {}_1F_1(i\xi, 1, -ikr - i\mathbf{k}\cdot\mathbf{r}) \tag{7}$$

is the Coulomb distortion, $N(\xi) = \exp(-\pi\xi/2)\Gamma(1 - i\xi)$ is the Coulomb factor, $\xi = -\mu Z/k$ is the Sommerfeld parameter, and μ is the reduced mass ($Z > 0$ for attractive potentials). As usual, we denote $\mathbf{r}_{12} = \mathbf{r}_1 - \mathbf{r}_2$, $\mathbf{k}_{12} = (\mathbf{k}_1 - \mathbf{k}_2)/2$, $\xi_1 = -Z_T/k_1$, $\xi_2 = -Z_T/k_2$, and $\xi_{12} = 1/(2k_{12})$. In Eq. (6), $\mathcal{P}_{12} = (1 + P_{12})/\sqrt{2}$, where P_{12} is the exchange operator.

As the separation of the three particles tends to infinity Eq. (6) adopts the form

$$\psi_f^-(\mathbf{k}_1, \mathbf{k}_2 | \mathbf{r}_1, \mathbf{r}_2) \longrightarrow \mathcal{P}_{12} \psi_{\mathbf{k}_1}^0(\mathbf{r}_1) \psi_{\mathbf{k}_2}^0(\mathbf{r}_2) e^{i\phi^-}, \tag{8}$$

$$\phi^-(\mathbf{k}_1, \mathbf{k}_2 | \mathbf{r}_1, \mathbf{r}_2) = -Z_T f^-(\mathbf{k}_1, \mathbf{r}_1) - Z_T f^-(\mathbf{k}_2, \mathbf{r}_2) + \tfrac{1}{2} f^-(\mathbf{k}_{12}, \mathbf{r}_{12}), \tag{9}$$

with $f^-(\mathbf{k}, \mathbf{r}) = -k^{-1} \ln(kr + \mathbf{k}\cdot\mathbf{r})$. Equations (8) and (9) are the correct asymptotic behavior of the three-body Coulomb wave function [8, 28].

By taking $\xi_{12} = 0$ in Eq. (6), the final state turns

TABLE I. Parameters for helium ground-state wave functions of Eq. (5). Values of correlation energy and cusp ratio are included.

Wave function	N_i	a	b	C_0	λ_0	$E_{\rm corr}$	$R_{\rm cusp}$
GS1	0.70892	2.1832	1.1885	0		33%	−1.685
GS2	1.63833	1.4096	2.2058	−0.6054	0.2420	96%	−1.807

out to be the independent-electron approximation, C2 in our notation, indicating the product of only two Coulomb waves. In this case the final state reduces to $\mathcal{P}_{12}\psi^-_{\mathbf{k}_1}(Z_T;\mathbf{r}_1)\psi^-_{\mathbf{k}_2}(Z_T;\mathbf{r}_2)$, which has been extensively used in double photoionization [21, 23, 29]. It should be pointed out that both the C3 and the C2 exactly satisfy the cusp condition at the nucleus.

Independently, a program [22] which uses multiconfigurational self-consistent-field wave functions for the initial state and a simple product of two Coulomb continua (C2 model) was developed in our group. This program has served as a permanent check for the present calculations. In particular, two initial states were employed: the GS1 (which has a multiconfigurational form [30]) and the SH wave function.

D. Numerical calculations

To calculate $\mathbf{T}^{(G)}_{fi}$ we first need to transform the function on $\mathbf{r}_{12}$ in the Fourier space and then integrate separately the functions on $\mathbf{r}_1$ and $\mathbf{r}_2$ leading to the following momentum-space integrals $\mathbf{J}_1$, $\mathbf{J}_2$, and $\mathbf{J}_3$ defined as

$$\begin{bmatrix}\mathbf{J}_1(a,b,z,Z_T;\mathbf{k}_1,\mathbf{k}_2)\\ \mathbf{J}_2(a,b,z,Z_T;\mathbf{k}_1,\mathbf{k}_2)\\ \mathbf{J}_3(a,b,z,Z_T;\mathbf{k}_1,\mathbf{k}_2)\end{bmatrix} = \int d\mathbf{p}\begin{bmatrix}g(\mathbf{p};z)\\ g(\mathbf{p};z)\\ \mathbf{h}(\mathbf{p};z)\end{bmatrix}\int\int d\mathbf{r}_1 d\mathbf{r}_2\begin{bmatrix}\hat{\mathbf{r}}_1\\ \mathbf{r}_1\\ 1\end{bmatrix}F_1F_2$$
$$\times\exp(-ar_1 - i\mathbf{k}_1\cdot\mathbf{r}_1 + i\mathbf{p}\cdot\mathbf{r}_1)\exp(-br_2 - i\mathbf{k}_2\cdot\mathbf{r}_2 - i\mathbf{p}\cdot\mathbf{r}_2), \tag{10}$$

where we use the notation $F_j =_1 F_1(-i\xi_j, 1, ik_jr_j + i\mathbf{k}_j\cdot\mathbf{r}_j)$,

$$\begin{bmatrix}g(\mathbf{p};z)\\ \mathbf{h}(\mathbf{p};z)\end{bmatrix} = \int d\mathbf{r}_{12}\exp(-i\mathbf{p}\cdot\mathbf{r}_{12} - zr_{12})\begin{bmatrix}1\\ \hat{\mathbf{r}}_{12}\end{bmatrix}F_{12}, \tag{11}$$

$z = \lambda_0$ in $\mathbf{h}(\mathbf{p};z)$, and $z\to 0^+$ or $z=\lambda_0$ in $g(\mathbf{p};z)$. Nordsieck integrals on $\mathbf{r}_1$, $\mathbf{r}_2$ and $\mathbf{r}_{12}$ have closed forms [31].

We have developed a program to numerically perform the present three-dimensional integrals on $\mathbf{p}$. The relative error of integration was set to be less than 1%. The task is quite cumbersome due to the pole at the origin $p=0$ in $g(\mathbf{p}, z=0)$, which can be removed if a cutoff z_c is introduced. The final result then requires the limit $z_c\to 0^+$. The calculations of total and single differential cross sections in the present work were done by setting $z_c = 0.005$. A total cross section demands about 20 h on a 10-Mflop Risc-technology computer.

The velocity matrix element is then given by

$$\begin{aligned}\mathbf{T}^{(V)}_{fi} = &-C\mathcal{P}_{12}[a\mathbf{J}_1(a,b,z_c,Z_T;\mathbf{k}_1,\mathbf{k}_2) + b\mathbf{J}_1(b,a,z_c,Z_T;\mathbf{k}_1,\mathbf{k}_2)\\ &+C_0a\mathbf{J}_1(a,b,\lambda_0,Z_T;\mathbf{k}_1,\mathbf{k}_2) + C_0b\mathbf{J}_1(b,a,\lambda_0,Z_T;\mathbf{k}_1,\mathbf{k}_2)\\ &+\lambda_0C_0\mathbf{J}_3(a,b,\lambda_0,Z_T;\mathbf{k}_1,\mathbf{k}_2) + \lambda_0C_0\mathbf{J}_3(b,a,\lambda_0,Z_T;\mathbf{k}_1,\mathbf{k}_2)],\end{aligned} \tag{12}$$

and $C = 2N_iN^*(\xi_1)N^*(\xi_2)N^*(\xi_{12})/(2\pi)^6$, where $N^*(\xi)$ is the complex conjugate of the Coulomb factor $N(\xi)$ defined below Eq. (7). A similar expression is obtained for the length form including only the $\mathbf{J}_2$ integral.

A fundamental test was made to assure the precision of our calculation of the numerical integration: by taking $\xi_{12}=0$ (C2) and using the GS1 wave function, then we can compare our numerical results with the independent program [22] mentioned before, which makes use of closed forms. As $z_c\to 0^+$ both programs must give the same result within the numerical accuracy (see Fig. 1).

We further study the convergence velocity of our results, as shown in Fig. 1, where we present one point of the FDCS as a function of z_c. By choosing $z_c = 0.005$, we expect relative errors of about 2% and 3%, if GS1 and GS2 initial wave functions are used, respectively. Summarizing, a total cross section presents a relative error of less than 5%, after a five-dimensional numerical integral (three dimensional on $\mathbf{p}$, θ_{12}, and ε_1), and the limit as z_c tends to zero.

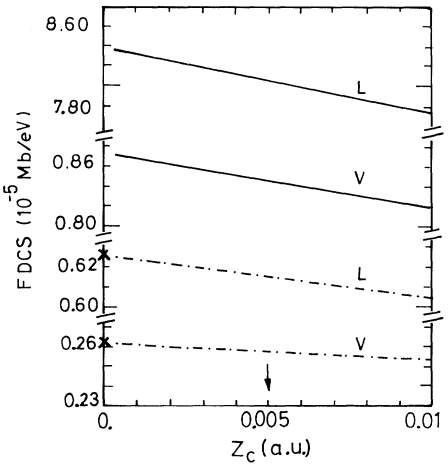

FIG. 1. FDCS as a function of z_c. The vectors $\mathbf{k}_1$, $\mathbf{k}_2$, and $\hat{\mathbf{e}} = \hat{\mathbf{z}}$ are coplanar. The electron energies are $\varepsilon_1 = \varepsilon_2 = 15$ eV, $\theta_1 = 90°$, and $\theta_2 = 0°$. Solid line: Initial state GS2 and C3 final state in the velocity (V) and length (L) forms. Dot-dashed line: Initial state GS1 and C3 final state with $\xi_{12}=0$. The crosses are the results obtained with GS1 initial state and C2 final state employing the independent program developed in Ref. [22]. The vertical arrow indicates the z_c value used in the calculations.

III. RESULTS

The electron kinetic-energy distributions in the velocity gauge for different photon energies are presented in Fig. 2 together with the experimental data [14] at $E_\gamma = 120$ eV. For completeness the C2 results using

the SH ground-state wave function are also included as the dot-dashed line. At lower energies, the theoretical shape does not agree with the experimental U-shaped form, indicating the inadequacy of the present approximation in this range. However, as the energy increases the expected U-shaped form is reached; at 1.0 keV the curve is parabolic. Notice, at 2.0 keV and higher energies the curve has a flat-top peak at the very center of the distribution. This feature has already been observed by Amusia *et al.* [32], and corresponds to the case where the wavelength of the photon is about the size of the atom. Notice, this structure is not present when using the C2 model, as shown in the figure.

For high photon energies, the leading contribution to the total cross section, when integrating the kinetic-energy distribution, comes from the regions of the spectrum where one electron escapes with almost all of the available energy, namely, $\varepsilon_1 \simeq 0$ and $\varepsilon_2 \simeq E_\gamma + E_0$, and vice versa. This implies $\xi_{12} = 1/|\mathbf{k}_1 - \mathbf{k}_2| \to 0$ and therefore the effect of the correlation, embodied in the multiplicative term $D^-(\xi_{12}, \mathbf{k}_{12}; \mathbf{r}_{12})$, tends to disappear, as seen in Fig. 2 for $E_\gamma = 3.0$ keV. This is the reason why our total cross sections including correlation would give the same high-energy limit as the C2 model if we used the same initial state.

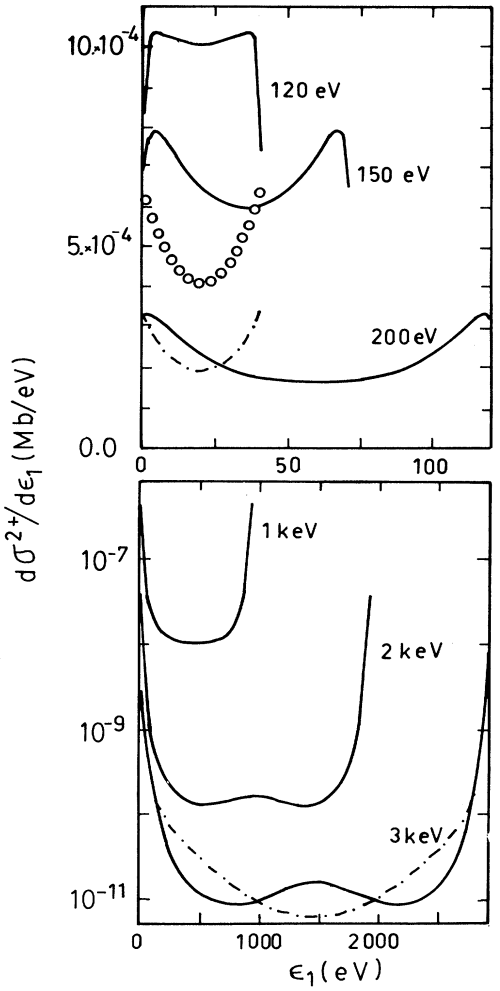

FIG. 2. Electron kinetic-energy distribution (velocity formulation) as a function of the energy of an electron employing wave functions GS2 and C3 for the initial and final states, respectively. The dot-dashed lines are the results employing SH and C2 states. Upper figure for $E_\gamma = 120$, 150, and 200 eV together with the experimental curve of Ref. [14] at 120 eV (empty circles). Lower figure for $E_\gamma = 1.0$, 2.0, and 3.0 keV.

Figure 3 shows the ratio of double- to single-ionization cross sections as a function of the photon energy in the length and velocity gauges together with available experimental data, covering from the threshold region [13] up to the recent high-energy synchrotron measurements [19, 20]. As single-ionization cross sections, we use the Coulomb approximation of Stewart and Webb [33] using the SH wave function for the initial state within the velocity gauge (see Table II).

Our results present a large length-velocity discrepancy in the whole range of energy investigated, the velocity form being the most appropriate for high energies, as predicted by Dalgarno and Sadeghpour [34]. These authors have shown that for large photon energies the error when using an approximate wave function in the length form remains unaltered whereas in the velocity and acceleration forms the error drops as E_γ^{-1} and E_γ^{-2}, respectively. The good behavior of our velocity formulation at high energy could be accounted for in this way.

At high energies, the velocity-gauge ratio tends to 1.75%, slightly differing from the asymptotic ratio 1.68% predicted by many workers [23, 26, 34]. This small difference can be attributed to both: first, a deficiency of initial-state wave function (for GS2, the cusp ratio is -1.807 instead of -2), and second, errors of integrations (estimated to be less than 5%). Accepting these short-

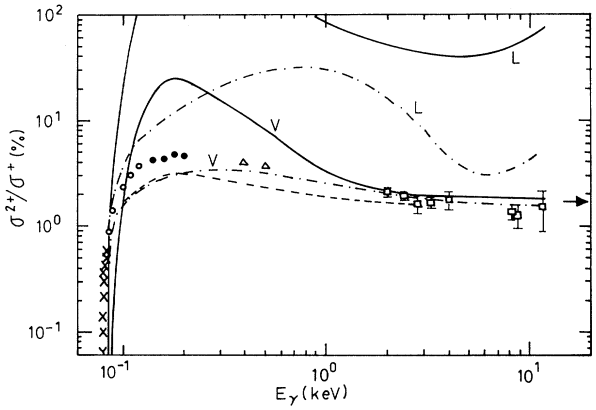

FIG. 3. Ratio $\sigma^{2+}/\sigma^{+}(\%)$ as a function of the photon energy. Solid line: calculations with GS2 and C3 for the initial and final states, respectively, in the velocity (V) and length (L) forms. Dot-dashed line: calculations with SH and C2 states. Dashed line: many-body perturbation theory (MBPT) calculations of Ref. [37]. Cross (×): experimental values of Ref. [13]. Empty circle (○): experimental values of Ref. [14]. Full circle (●): experimental values of Ref. [16]. Triangle (△): experimental values of Ref. [17]. Square (□): experimental values of Refs. [19, 20]. The arrow indicates the asymptotic limit 1.68% obtained in Refs. [23, 26, 34].

TABLE II. Total cross sections in the velocity gauge of single and double ionization of helium by photons of energy E_γ. σ^+, single-photoionization cross sections in the Coulomb approximation [33] using the SH initial state; σ^{2+}_{C2}, double-photoionization cross sections using SH and C2 states; and σ^{2+}_{C3}, double-photoionization cross sections using GS2 and C3 states.

E_γ (keV)	σ^+ (Mb)	σ^{2+}_{C2} (Mb)	σ^{2+}_{C3} (Mb)
0.084	5.41×10^{-1}	2.84×10^{-3}	2.3×10^{-5}
0.1	3.48×10^{-1}	5.44×10^{-3}	6.2×10^{-3}
0.12	2.17×10^{-1}	4.86×10^{-3}	2.0×10^{-2}
0.15	1.19×10^{-1}	3.30×10^{-3}	2.4×10^{-2}
0.2	5.44×10^{-2}	1.69×10^{-3}	1.3×10^{-2}
0.5	3.74×10^{-3}	1.17×10^{-4}	3.1×10^{-4}
1.0	4.24×10^{-4}	1.06×10^{-5}	1.3×10^{-5}
2.0	4.40×10^{-5}	8.95×10^{-7}	9.2×10^{-7}
3.0	1.13×10^{-5}	2.02×10^{-7}	2.2×10^{-7}
4.0	4.31×10^{-6}	7.16×10^{-8}	8.1×10^{-8}
6.0	1.09×10^{-6}	1.75×10^{-8}	2.0×10^{-8}
8.0	4.08×10^{-7}	6.54×10^{-9}	7.4×10^{-9}
10.0	1.90×10^{-7}	3.04×10^{-9}	3.4×10^{-9}
12.0	1.02×10^{-7}	1.63×10^{-9}	1.8×10^{-9}

comings, our limit is consistent with previous results [23, 26, 34].

The C2 results using the SH initial state produce a high-energy ratio of 1.60% which also slightly deviates from the value 1.68%, due probably to the deficit of the cusp condition. Both velocity calculations, employing C3 and C2, reached the asymptotic limit at about $E_\gamma = 4.0$ keV, in accordance with Levin *et al.*'s result [20].

As was observed by Byron and Joachain [23] $\sigma^{2+(L)}_{C2} \to E_\gamma^{-5/2}$ and as $\sigma^{+(V)} \to E_\gamma^{-7/2}$ the ratio in the length form increases linearly as $E_\gamma \to \infty$ as shown in Fig. 3; our ratio using the C3 wave function also behaves linearly as $E_\gamma \to \infty$ (see Fig. 3), therefore we can infer that $\sigma^{2+(L)}_{C3} \to E_\gamma^{-5/2}$.

At intermediate energies, the calculated ratio is up to five times larger than the data. At lower photon energies the theory runs well below the data; for example, at $E_\gamma =$ 84 eV the theory gives a ratio of 0.004% while the data is 0.6% [14].

IV. CONCLUDING REMARKS

We have applied a correlated double-continuum wave function to study double photoionization. A large length-velocity discrepancy is observed in the whole range of energy investigated (from threshold to 12 keV), although the velocity form tends to the correct asymptotic limit. The correlated final wave function C3 works for photon energies larger than 1 keV. At lower energies, substantial deficiencies are observed not only at the level of the total cross section, but also at the level of electron energy distributions.

The C3 wave function has been extensively used in electron-atom collisions and in this work it is firmly tested, since the initial state used here accounts for most of the correlation. A direct reading shows the deficiencies of the C3 final state for available electron energies less than 1 keV. And this is not a problem of normalization alone, since at $E_\gamma = 120$ eV it fails also to account for the *shape* of the experiments.

The C3 wave function and related functions have been used in electron-atom collision to explain the Wannier mechanisms in the threshold region [35]. Further, even in the context of double photoionization the C3 wave function has been used to calculate the asymmetry parameter β [12]. In both cases, the theory accounts quite well for the shape of the experiments in arbitrary units. However, in our case, we find that in the low-energy region the validity of the C3 state worsens, underestimating the data by orders of magnitude. Anyway, the deficiencies of the C3 wave function for low available electron energies should be taken with cautions; in this context, Kamber *et al.* [36] have claimed that the photoionization calculation probes the wave functions in a region of momentum space different from that addressed in charged-particle impact.

ACKNOWLEDGMENTS

We thank Dr. Ralf Wehlitz for providing us with the experimental data, and Jim McGuire for useful discussions during his visit to our Institute.

[1] J. H. McGuire, Adv. At. Mol. Opt. Phys. **29**, 217 (1991).
[2] R. J. Tweed, J. Phys. B **6**, 270 (1973).
[3] M. Schulz, J. Phys. B **6**, 2580 (1973).
[4] A. Huetz, P. Selles, D. Waymel, and J. Mazeau, J. Phys. B **24**, 1917 (1991).
[5] P. L. Altick, Phys. Rev. A **21**, 1381 (1980); **25**, 128 (1982); J. Phys. B **16**, 3543 (1983); **18**, 1841 (1985).
[6] L. Vainshtein, L. Presnyakov, and I. Sobelman, Zh. Eksp. Teor. Fiz. **45**, 2015 (1963) [Sov. Phys. JETP **18**, 1383 (1964)].
[7] C. R. Garibotti and J. E. Miraglia, Phys. Rev. A **21**, 572 (1980).
[8] M. Brauner, J. S. Briggs, and H. Klar, J. Phys. B **22**, 2265 (1989).
[9] M. Brauner, J. S. Briggs, and J. T. Broad, J. Phys. B **24**, 287 (1991).
[10] M. Brauner, J. S. Briggs, H. Klar, J. T. Broad, T. Rossel, K. Jung, and H. Ehrhardt, J. Phys. B **24**, 657 (1991).
[11] B. Joulakian, C. Dal Cappello, and M. Brauner, J. Phys. B **25**, 2863 (1992).
[12] F. Maulbetsch and J. S. Briggs, Phys. Rev. Lett. **68**, 2004 (1992).
[13] H. Kossmann, V. Schmidt, and T. Andersen, Phys. Rev. Lett. **60**, 1266 (1988).
[14] R. Wehlitz, F. Heiser, O. Hemmers, B. Langer, A. Menzel, and U. Becker, Phys. Rev. Lett. **27**, 3764 (1991).
[15] V. Schmidt, N. Sandner, and H. Kuntzemuller, Phys. Rev. A **13**, 1748 (1976).

[16] D. M. P. Holland, K. Codling, J. B. West, and G. V. Marr, J. Phys. B **12**, 2465 (1979).
[17] J. A. R. Samson, R. J. Bartlett, and Z. X. He, Phys. Rev. A 46, 7277 (1992).
[18] T. A. Carlson, Phys. Rev. **156**, 142 (1967).
[19] J. C. Levin, D. W. Lindle, N. Keller, R. D. Miller, Y. Azuma, N. Berrah Mansour, H. G. Berry, and I. A. Sellin, Phys. Rev. Lett. **67**, 968 (1991).
[20] J. C. Levin, I. A. Sellin, B. M. Johnson, D. W. Lindle, R. D. Miller, N. Berrah, Y. Azuma, H. G. Berry, and D.-H. Lee, Phys. Rev. A **47**, R16 (1993).
[21] H. Le Rouzo and C. Dal Cappello, Phys. Rev. A **43**, 318 (1991).
[22] V. D. Rodríguez, M. A. Kornberg, and C. A. Falcón, in *Collision Processes of Ion, Positron, Electron and Photon Beams with Matter, Proceedings of the Latin American School of Physics, Caxambu, Brazil, 1991*, edited by C. A. C. Souza *et al.* (World Scientific, Singapore, 1992), pp. 437–446.
[23] M. E. Rose, *Elementary Theory of Angular Momentum* (Wiley, New York, 1957), p. 50.
[24] R. A. Bonham and D. A. Kohl, J. Chem. Phys. **45**, 2471 (1966).
[25] F. W. Byron and C. J. Joachain, Phys. Rev. A **164**, 1 (1967).
[26] T. Åberg, Phys. Rev. A **2**, 1726 (1970).
[27] N. Sabelli and J. Hinze, J. Chem. Phys. **50**, 648 (1969).
[28] L. Rosenberg, Phys. Rev. D **8**, 1833 (1973).
[29] R. L. Brown, Phys. Rev. A **1**, 586 (1970).
[30] J. N. Silverman, O. Platas, and F. A. Matsen, J. Chem. Phys. **32**, 1402 (1960).
[31] M. S. Gravielle and J. E. Miraglia, Comput. Phys. Commun. **69**, 53 (1992).
[32] M. Ya Amusia, E. G. Drukarev, V. G. Gorshkov, and M. P. Kazachkov, J. Phys. B **8**, 1248 (1975).
[33] A. L. Stewart and T. G. Webb, Proc. Phys. Soc. London **82**, 532 (1963).
[34] A. Dalgarno and H. R. Sadeghpour, Phys. Rev. A **46**, R3591 (1992).
[35] J. Botero and J. H. Macek, Phys. Rev. Lett. **68**, 576 (1992).
[36] E. Y. Kamber, C. L. Cocke, S. Cheng, and S. L. Varghese, Phys. Rev. Lett. **60**, 2026 (1988).
[37] T. Ishihara, K. Hino, and J. H. McGuire, Phys. Rev. A **44**, R6980 (1991).